



CHALMERS
UNIVERSITY OF TECHNOLOGY

Effects of port-fuel injected methanol distribution on cylinder-to-cylinder variations in a retrofitted heavy-duty diesel–methanol dual fuel engine

Downloaded from: <https://research.chalmers.se>, 2025-04-04 09:30 UTC

Citation for the original published paper (version of record):


Mousavi, S., Tripathy, S., Molander, P. et al (2025). Effects of port-fuel injected methanol distribution on cylinder-to-cylinder variations in a retrofitted heavy-duty diesel–methanol dual fuel engine. *Fuel*, 391. <http://dx.doi.org/10.1016/j.fuel.2025.134733>

N.B. When citing this work, cite the original published paper.



Full length article

Effects of port-fuel injected methanol distribution on cylinder-to-cylinder variations in a retrofitted heavy-duty diesel–methanol dual fuel engine

Seyed Morteza Mousavi ^a ,* , Srinibas Tripathy ^a , Patrik Molander ^b , Petter Dahlander ^a

^a Department of Mechanics and Maritime Sciences, Chalmers University of Technology, Gothenburg SE-412 96, Sweden

^b ScandiNAOS AB, Gothenburg SE-414 51, Sweden

ARTICLE INFO

Keywords:

Diesel–methanol dual fuel
PFI
Methanol fumigation
CFD

ABSTRACT

A 6-cylinder, 13-litre diesel engine was converted to operate on a combination of port-fuel-injected (PFI) methanol and direct-injected (DI) diesel as the pilot fuel. This conversion presents significant challenges, particularly in the design of the inlet manifold, due to inevitable methanol mass imbalances between cylinders that must be minimized. This study integrates experimental and numerical methods to investigate methanol distribution in the retrofitted, non-EGR marine diesel engine. The focus is on cylinder-to-cylinder variations caused by uneven methanol distribution. Two in-cylinder pressure sensors were employed to measure and compare pressure in the second and sixth cylinders. Results indicate that increasing the methanol energy fraction (MEF) at each test point intensifies the differences between the pressure traces in the two cylinders. To delve into this phenomenon, a computational fluid dynamics (CFD) model was developed to explore the behavior of the inlet manifold and the PFI system. Additionally, shadowgraphy experiments were conducted in an optical spray chamber to validate the CFD model. Analysis based on the model suggests that cylinder-to-cylinder variation stems from uneven fuel distribution between cylinders. Calculations reveal that the difference in the mass of methanol across cylinders can reach up to 18% at high MEFs, consistent with experimental findings. Furthermore, a novel design for the inlet manifold was devised and simulated, demonstrating a marked enhancement in fuel distribution. The revised design effectively reduces the fuel mass imbalance to 3%, with the remaining slight imbalance caused by gaseous fuel accumulation at the end of the inlet manifold. Finally, simulations were performed to scrutinize the impact of injection timing, injection duration, and injector location on fuel mass distribution imbalance. The results show that while the manifold design is the most important parameter affecting the fuel distribution, the PFI location and settings can also be adjusted to mitigate the fuel distribution problems.

1. Introduction

The concerns regarding air pollution, global warming, and energy security have sparked a global quest to find fossil fuel alternatives, especially in the transport sector. Among these alternatives, alcohols and methanol (CH₃OH) in particular, have emerged as promising fuels for internal combustion engines (ICEs). While methanol has a long history as a fuel since the inception of ICEs, its popularity has surged in recent years, driven by soaring oil prices, a deeper understanding of climate changes, and new environmental regulations [1]. Methanol offers several advantages: it can be derived from biomass and renewable sources, boasts a minimal environmental footprint, is versatile enough to be used as a standalone fuel or blended, produces no soot, exhibits properties akin to gasoline, and is more cost-effective than other alcohols like ethanol [2,3]. Despite restrictions on ICEs in road

vehicles, methanol combustion holds promise as a viable solution for marine applications [4,5]. Consequently, exploring the potential of methanol in both new and existing marine engines is an intriguing prospect.

Various approaches exist for integrating methanol into internal combustion engines (ICEs). Methanol has a high octane (low cetane) number similar to gasoline, which makes it compatible with spark ignition (SI) engines [6]. However, the high octane number renders methanol unsuitable for direct use in compression ignition (CI) engines, renowned for their superior thermal efficiency among combustion engines. Nonetheless, methanol addresses the primary drawbacks of CI engines, namely, soot and NO_x emissions. Modifying an existing diesel engine to enhance its compatibility with methanol is possible. One potential solution for incorporating methanol into CI engines is

* Corresponding author.

E-mail address: morteza.mousavi@chalmers.se (S.M. Mousavi).

<https://doi.org/10.1016/j.fuel.2025.134733>

Received 9 July 2024; Received in revised form 7 October 2024; Accepted 12 February 2025

Available online 21 February 2025

0016-2361/© 2025 The Authors. Published by Elsevier Ltd. This is an open access article under the CC BY license (<http://creativecommons.org/licenses/by/4.0/>).

the diesel–methanol dual-fuel (DMDF) operation, in which diesel acts as a pilot fuel to ignite the methanol. Various approaches to DMDF operation are briefly discussed in the following.

In a DMDF engine, methanol can be blended with diesel and directly injected into the cylinder, with or without the addition of an emulsifier. This method necessitates minimal modifications to the existing CI engine, but the proportion of methanol that can be blended with diesel is limited. Methanol has low solubility in diesel, and even with the addition of emulsifiers, no more than 25% of diesel can be replaced by methanol effectively in the fuel blend [3]. Alternatively, a more complex approach involves direct injection of methanol and direct injection of diesel (DI-DI), as the primary and pilot fuels, respectively [7,8]. However, this technique entails installing an additional injector on top of each cylinder and modifying the cylinder head, posing challenges for certain engines. A third option is port fuel injection (PFI) of methanol, which can be ignited by pilot diesel directly injected into the cylinder. Referred to as alcohol fumigation, this method is the prevalent approach for adapting a conventional diesel engine and forms the primary focus of this paper.

PFI was the common practice in gasoline engines [9], but in recent decades, methanol fumigation coupled with direct diesel injection has emerged as an effective strategy to enhance diesel engine performance [10,11]. Generally, methanol fumigation can result in reduced diesel consumption, as well as lower CO₂, NO_x, and soot emissions, albeit with higher CO and hydrocarbon (HC) emissions compared to conventional diesel combustion [10,12,13]. Methanol lacks carbon-to-carbon bonds and does not generate soot, and its high heat of evaporation contributes to lower combustion temperatures and reduced NO_x emissions [1,10,14]. An oxidation catalyst can mitigate the elevated HC and CO emissions associated with methanol fumigation, particularly at lower loads [14–16].

In recent years, various factors influencing the performance and emissions of DMDF mode have been explored. Pan et al. [17] delved into the impact of intake air temperature on a 6-cylinder turbocharged heavy-duty (HD) engine. Their study revealed that elevated intake temperature enhances indicated thermal efficiency, and triggers earlier ignition and higher peak cylinder pressure, while also reducing HC and CO emissions. This effect becomes more pronounced at higher methanol fractions. Meanwhile, Wang et al. [18,19] conducted research using the same engine to probe the boundaries of engine operation and cyclic variability with methanol fumigation. Their findings outlined four limiting factors: partial burning at low loads, misfire at medium loads, and roar combustion and knock at higher loads. They achieved a maximum methanol substitution of 76% at approximately 35% load [18]. Additionally, they noted that DMDF operation at higher loads or intake temperatures exhibits greater combustion stability (lower cyclic variability) [19], potentially leading to enhanced brake thermal efficiency (BTE) [20]. Moreover, Duraisamy et al. [21] explored DMDF in a 3-cylinder, light-duty turbocharged diesel engine, revealing reduced cycle-to-cycle variation at high loads. Furthermore, their results demonstrated that 26% cooled exhaust gas recirculation (EGR) resulted in diminished cycle-to-cycle variation, lower NO_x and soot emissions, and heightened thermal efficiency.

Another critical parameter influencing the performance of a DMDF engine is the fuel injection strategy. While the effects of diesel injection timing and pressure on conventional diesel engines are well-documented, recent studies have further investigated their implications for CI engines with methanol fumigation [22,23]. Additionally, the impact of the PFI strategy on engine performance has garnered attention and requires further examination [24–27]. Chen et al. [24] explored the effect of different methanol injector positions on cylinder-to-cylinder and cycle-to-cycle variations in a turbocharged inline 4-cylinder engine. They tested three injection positions: one injector at the intake port of each cylinder, all injectors far upstream of the inlet manifold, and all injectors in one point close to the inlet manifold. The first and second cases exhibited relatively low cylinder-to-cylinder variation, whereas

Table 1
Test engine specification.

Configuration	In-line, 6 cylinders
Valve configuration	4 valves per cylinder
Compression ratio	17:1
Displacement	12.8 L
Cylinder bore	131 mm
Stroke	158 mm
Connecting rod length	267.5 mm
Diesel injection system	Common rail DI

the third case showed high variation, especially at high methanol energy fractions (MEF). Xu et al. [25,26] observed lower HC and CO emissions for pre-intercooler methanol injection compared to post-intercooler injection. Lastly, Dierickx et al. [27] compared single-point injection (SPI) at the inlet duct to multiple-point injection (MPI) at the intake ports of each cylinder. They concluded that SPI, being easier to install and leading to higher BTE, is preferred from a cost perspective. Conversely, MPI provides additional cylinder cooling to prevent knock, maximizes MEF, and minimizes NO_x emissions, making it preferable from a sustainability standpoint.

Recent studies on methanol injection strategies have addressed some of the primary challenges associated with retrofitting specific types of diesel engines. However, different engine types and inlet manifold designs necessitate varied solutions to achieve optimal DMDF operation. Therefore, further research is needed to pinpoint the key parameters influencing engine performance when integrating methanol injectors into existing diesel engines. Additionally, while current computational fluid dynamics (CFD) simulations of DMDF engines focus on combustion within a single cylinder [1], there is potential to conduct CFD simulations of the airflow and fuel distribution inside the inlet manifold and multiple cylinders. Such a model could facilitate the study and enhancement of the methanol PFI injection system.

In this study, a Volvo D13 6-cylinder turbocharged HD diesel engine is retrofitted to operate in DMDF mode. Six methanol injectors are installed at the rear side of the inlet manifold, directed toward the intake port of each cylinder. Significant substitution of diesel with methanol is achieved at various loads. However, an elevated cylinder-to-cylinder variation is observed with increasing MEF. Consequently, a CFD model is developed to address this issue, focusing on analyzing the airflow and methanol distribution within the inlet manifold. Shadowgraphy experiments conducted in a spray chamber yield data for validating the spray model. Furthermore, the CFD predictions regarding cylinder-to-cylinder variation are compared against engine measurements. The validated CFD model guides the development of an enhanced design for the inlet manifold and injectors, effectively mitigating cylinder-to-cylinder variations. Finally, the numerical model is employed to examine the impact of injection timing, duration, and injector placement on fuel mass distribution across different cylinders.

2. Experimental measurements

2.1. Diesel engine

A six-cylinder four-stroke 13 L diesel engine is used in this study for diesel–methanol dual-fuel operation and performance investigations. The schematic of dual-fuel engine used in this study is shown in Fig. 1, and the engine specifications are presented in Table 1.

The diesel engine underwent modifications to enable diesel–methanol dual-fuel operation. This involved replacing the conventional intake manifold with a new one capable of accommodating six methanol injectors. Methanol injection occurred in the intake manifold, with the injection pressure adjustable between 3 and 10 bar. To facilitate methanol supplementation, an AVL fuel balancing and conditioning unit was utilized, ensuring precise control over methanol inlet temperature. Timing and duration of methanol injection during engine

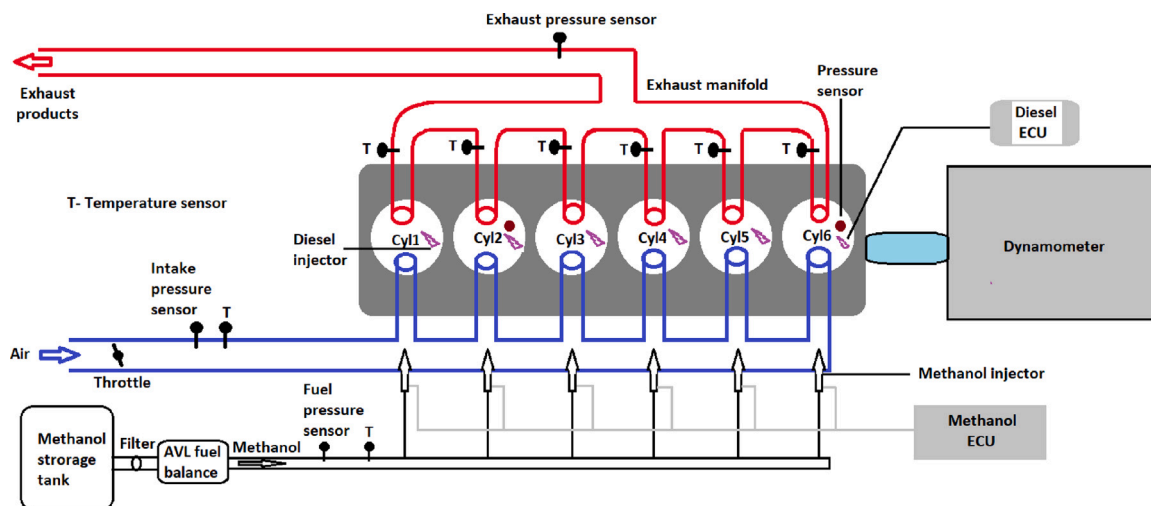


Fig. 1. Schematic of diesel–methanol dual-fuel engine experimental setup.

operation were managed by an open ECU. Additionally, a fuel pressure control valve was employed to regulate methanol injection pressure.

The multi-cylinder engine is fitted with an eddy current dynamometer for torque measurement, with a maximum capacity of 4000 N m. To investigate cylinder-to-cylinder performance and combustion variations in dual-fuel operation, it is ideal to install pressure sensors in all cylinders. However, this is both practically challenging and costly. Consequently, pressure sensors were mounted on cylinders 2 and 6 for in-cylinder pressure measurement. Cylinder 2 was chosen due to its high temperature, while cylinder 6 was selected for being farthest from the air inlet.

For in-cylinder pressure measurements, piezoelectric pressure transducers were employed, generating charge that was then amplified to voltage in a charge amplifier and calibrated to pressure. The peak cylinder limit for this engine stands at 200 bar. Intake and exhaust pressure and temperature measurements were facilitated by various sensors installed in the respective manifolds.

Diesel fuel injection was managed by a closed ECU, automatically adjusting injection pressure and timings based on calibrated inputs and demanded torque. A turbocharger was utilized during high-load operation to regulate intake and exhaust pressures. Additionally, an NI controller was employed to extract the diesel pilot and main fuel injection mass and timings during engine operation. A Labview based data acquisition software (Dewesoft) was used for acquiring the in-cylinder pressures as well as intake and exhaust pressures and temperatures at different points.

Dual-fuel operation is investigated at different test points ranging from low load to high point operation. At each operating point, the measurements started by running the engine on pure diesel, and the methanol amount was gradually increased while monitoring the combustion stability and keeping the coefficient of variation (COV) of integrated mean effective pressure (IMEP) below 5%.

To meet the objectives of this study, two test points relevant to marine applications (close to 50% and 75% load on the propeller curve) were selected to illustrate cylinder-to-cylinder variations. The operating conditions of these test points (TP1 and TP2) and the maximum MEF achieved with the engine's stock settings are outlined in Table 2. Throughout the paper, different cases are addressed using a combination of test number and MEF value. For instance, TP1-MEF40 refers to Test Point 1 at an MEF of 40%.

Other than the experiments on the engine, Shadowgraphy experiments were carried out in an optical chamber for spray characterization of the PFI injector, which helps in CFD model validation.

Table 2

Experimental conditions for different test points.

Case	Speed [rpm]	Torque [N m]	BMEP [bar]	Max MEF [%]
TP1	1638	1403	13.8	40
TP2	1234	875	8.6	60

2.2. Methanol spray shadowgraphy

In order to develop a realistic model of methanol injection in the PFI system, it is crucial to have data on parameters like spray cone angle, spray tip velocity, and discharge coefficient. While such information is readily available for various direct injectors, data for port fuel injectors are limited. Therefore, we conducted shadowgraphy experiments at different injection and chamber pressures to evaluate the spray characteristics.

The experimental setup and equipment used in the spray chamber measurements are illustrated in Fig. 2. The spray chamber's external dimensions are 30 × 20 × 20 cm, featuring four circular transparent windows with an 8 cm diameter on each side. At the top of the spray chamber is the methanol injector, specifically the Injector Dynamics ID1050x-60-14, commonly used in motorsport engines.

A mild airflow inside the chamber was necessary to prevent the accumulation of methanol. Two valves were employed to regulate airflow and air pressure within the chamber. Maintaining airflow at a low level (below 3000 L/h) in all cases was crucial to minimize interference with spray velocity.

Lighting was provided by a 250 W Dedocool Cool T3 Xe lamp positioned behind the spray chamber to create shadows of the spray droplets. For capturing spray shadow images, a Phantom v7.1 high-speed camera with a frame rate of 14035 Hz and a resolution of 256 × 512 pixels was utilized.

Data collection and synchronization of the injector trigger signal were managed by a National Instrument Corp. Compact RIO-9022, along with a program in LabView software. Injection pulse length and current were recorded using the data acquisition software (Dewesoft).

3. Numerical modeling

CFD simulations of air and methanol flow in the engine's inlet manifold were conducted using the commercial software Converge 3.0 [28]. The governing equations of gas-phase fluid flow, methanol spray modeling, and details regarding the numerical domain and boundary conditions are explained in the subsequent sections.

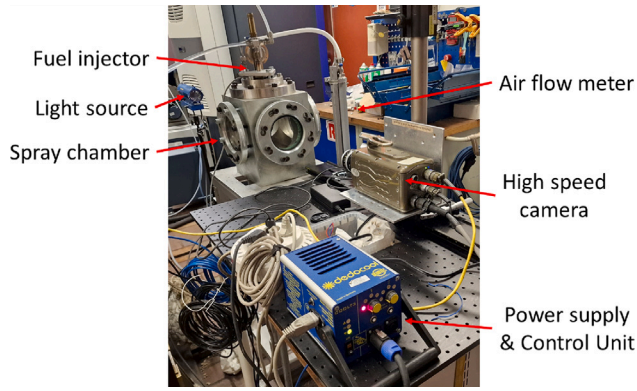


Fig. 2. Experimental equipment and arrangement for measurements in the spray chamber.

3.1. Governing equations

The continuity and momentum equations for the compressible, turbulent gas flow can be expressed in the form of

$$\frac{\partial \rho}{\partial t} + \nabla \cdot (\rho U) = \mathfrak{R}_p \quad (1)$$

and

$$\frac{\partial}{\partial t} (\rho U) + \nabla \cdot (\rho U U) = -\nabla p + \rho g + \nabla \cdot \tau - S_p, \quad (2)$$

where the total stress tensor, τ , is

$$\tau = \mu_{eff} \left[(\nabla U + \nabla U^T) - \frac{2}{3} \nabla \cdot U I \right]. \quad (3)$$

In the above equations, ρ , U , and p are the density, velocity, and pressure of the gas, respectively, and g is the gravitational acceleration. \mathfrak{R}_p is the mass source due to the evaporation of droplets, and S_p is the momentum source from the liquid droplets acting on the gas phase. μ_{eff} is the effective viscosity, which is the sum of the dynamic and turbulent viscosity of the gas phase.

The transport equations for species and energy are expressed in the form of

$$\frac{\partial}{\partial t} (\rho Y_i) + \nabla \cdot (\rho U Y_i) = \nabla \cdot (\rho D_{i,eff} \nabla Y_i) + \mathfrak{R}_i, \quad (4)$$

and

$$\begin{aligned} \frac{\partial}{\partial t} (\rho h) + \nabla \cdot (\rho U h) + \frac{\partial}{\partial t} (\rho K_e) + \nabla \cdot (\rho U K_e) - \frac{\partial p}{\partial t} \\ = \nabla \cdot (\alpha_{eff} \nabla h) + \dot{Q}_{d,conv}, \end{aligned} \quad (5)$$

where Y_i is the mass fraction of species i , h is the specific enthalpy of the mixture, and K_e is the kinetic energy per unit mass. $D_{i,eff}$ and α_{eff} are the effective diffusivity of species and effective thermal diffusivity of the mixture, respectively, which are calculated by a turbulence model similar to μ_{eff} . The single-species diffusion is calculated based on the transport data of each species. \mathfrak{R}_i is the species production term and $\dot{Q}_{d,conv}$ is the heat convection from droplets to the gas phase. In the present study, we only consider air (N_2 and O_2) and methanol in the simulations and combustion is not included in the model, so the only source term for species production is from the methanol droplet evaporation. Moreover, radiative heat transfer is neglected due to the relatively low temperature in the inlet manifold which is the main focus of this work. The Redlich-Kwong equation of state is used to couple the density and pressure fields and to close the system of equations.

3.2. Methanol spray

The main focus of this work is on the methanol distribution in different cylinders, which highlights the significance of methanol spray

modeling. On the other hand, the combustion inside the cylinders is not investigated, therefore the diesel spray is not modeled.

To model the methanol spray, six injectors positioned in front of each cylinder intake are added to the model. The start of injection (SOI), injected mass, and injection duration are determined based on experimental measurements for each case. Droplets are tracked in a Lagrangian frame of reference, with 5000 parcels introduced to the simulation per injection from each nozzle. The fuel temperature is maintained constant at 293 K across all cases.

The injectors produce a cone-shaped spray with a 10-degree cone half-angle. A blob size distribution is utilized, ensuring that the injected droplet size matches the diameter of the nozzle [28], which is approximately 1.75 mm in this study.

The Taylor Analogy Breakup (TAB) is used to calculate droplet distortion and drag coefficients which are important for accurate droplet modeling [29]. Kelvin–Helmholtz (KH) and Rayleigh–Taylor (RT) instability mechanisms are used to model spray atomization and breakup. Finally, the Frossling model is employed for droplet evaporation [30].

The spray is presumed to create a film layer over the wall, modeled by the O'Rourke film splash model [31]. Additionally, film evaporation is incorporated into the model. In the simulations conducted in this study, the majority of droplets impact the walls only after entering the intake ports of the cylinders. Consequently, the selection of the wall film model minimally affects the simulation objective, which is to estimate the amount of methanol entering each intake port.

3.3. Inlet manifold designs and numerical domain

To investigate cylinder-to-cylinder variations, the numerical domain includes the inlet manifold and all six cylinders. Two distinct designs of the inlet manifold are analyzed, as shown in Fig. 3. For simplicity, cylinders are denoted C_1 through C_6 , with C_1 representing the cylinder nearest to the intake.

Design 1 replicates the engine geometry, with injectors positioned at the back side of the inlet manifold. Simulations of this design serve to validate the CFD model and elucidate cylinder-to-cylinder variations observed in experiments.

Design 2 presents a conceptual approach aimed at mitigating cylinder-to-cylinder variations. In this design, the inlet manifold is shifted 8 cm from its original position and connected to cylinder ports through six connector pipes. Methanol injectors for cylinders C_2 to C_6 are located atop the connector pipes, angled toward the inlet valves. The injector angle for C_1 differs due to the mechanical constraints of the engine setup. CFD simulations of Design 2 were conducted to assess the significance of the inlet manifold and PFI system design on engine cylinder-to-cylinder variations.

3.4. Mesh and boundary conditions

A fully automatic mesh generation technique within the Converge software is adopted based on a pre-defined global base grid size. To study the sensitivity of simulation results to grid size, both a medium and a fine grid are generated, with base grid sizes of 4 mm and 3 mm, respectively. The comparison of two crucial parameters in this study — the air mass flow rate at the inlet and the mass of liquid and gas phase methanol entering cylinder C_6 over five consecutive cycles — is depicted in Fig. 4.

In both cases, the engine operates at 1638 rpm with a relatively high methanol injection mass of 132 mg per injector per cycle. Adaptive mesh refinement is implemented based on velocity and temperature gradients, with local refinements applied at spray locations, in proximity to valves, and adjacent to the cylinder head. Consequently, the number of grid cells fluctuates over time, but on average, the medium and fine meshes comprise approximately 1.4 million and 3.4 million cells, respectively.

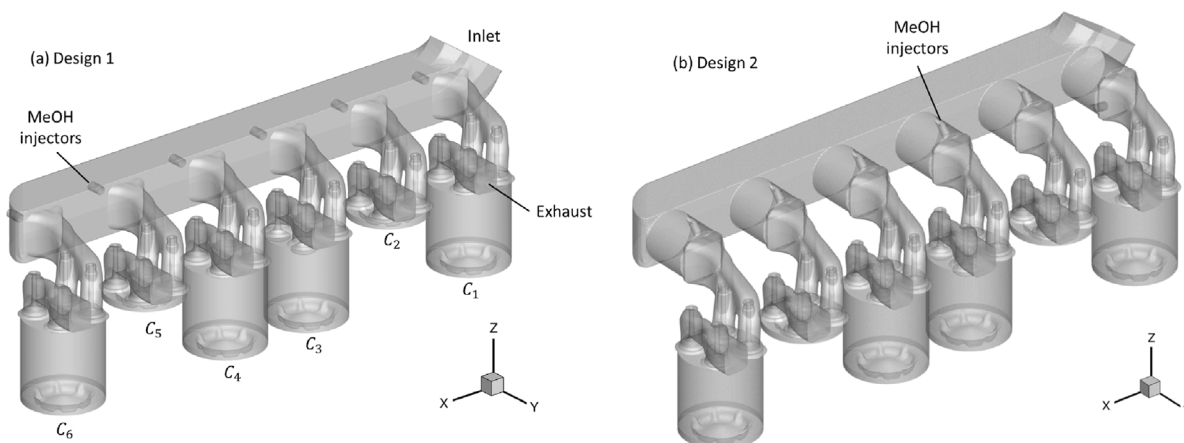


Fig. 3. Numerical domain including the inlet manifold and the six cylinders at CAD = 0. (a) Design 1, based on the engine geometry in the experiments, and (b) Design 2, proposed to improve the PFI fuel delivery.

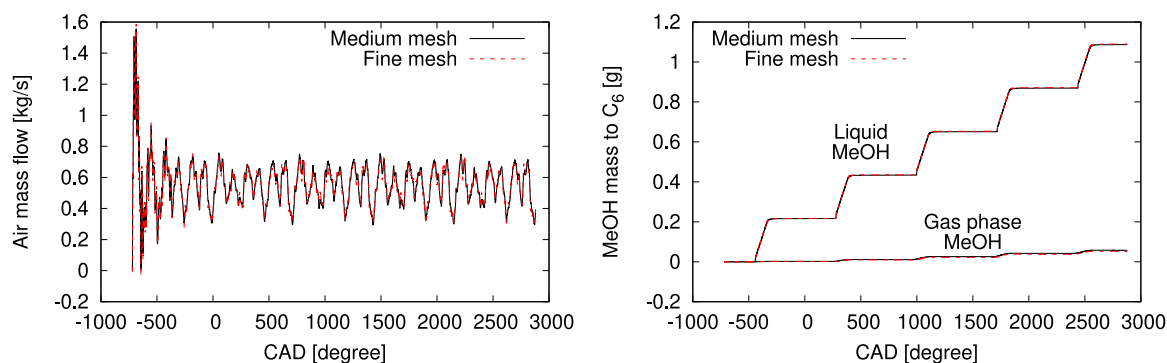


Fig. 4. Comparison of simulation results with medium and fine mesh. (a) Total mass flow of air at the inlet boundary and (b) liquid and gas phase methanol to C_6 .

As shown in Fig. 4, the results obtained with the two grids exhibit considerable similarity. Therefore, the medium mesh is employed for the remainder of this study.

The engine speed, injected methanol mass flow, and inlet pressure and temperature are determined from experimental measurements for various cases. In all cases, the wall temperature of the inlet manifold and intake ports is set to the measured air temperature within the inlet manifold. Piston movement is simulated according to the engine speed, while valve movements are based on profiles provided by the engine manufacturer.

Initial temperature and pressure in different domain regions — including the inlet manifold and intake ports, cylinders, and exhaust ports — are estimated from prior multi-cycle simulations of the engine at the same speed.

4. Results and discussion

In the subsequent sections, we delve into the experimental measurements on the engine, revealing significant cylinder-to-cylinder variations in DMDF mode. Following that, we present experimental data from the spray chamber used to validate the CFD model. Subsequently, we discuss numerical simulations of port-fuel injection in two different designs of the inlet manifold and compare the results. Lastly, we explore the effects of various parameters, including injection timing and duration, as well as injector position, on fuel delivery to different cylinders.

4.1. Experimental measurements on the engine

During DMDF operation, the engine underwent testing at various speeds and loads. At each test point, measurements commenced with

the engine running on pure diesel (MEF = 0). Then, the MEF was gradually increased until combustion and engine operation became unstable. It was observed that the knock intensity at high loads limits the MEF amount, which is consistent with earlier studies [18]. Despite the high octane number of methanol, adding more methanol increases the mixture's equivalence ratio, increasing the flame speed, the chances of auto-ignition, and the maximum pressure rise rate (PRR) at the high pressure and temperature corresponding to high load. An uneven fuel distribution between cylinders leads to more methanol in C_6 , further limiting the maximum MEF.

The pressures in C_2 and C_6 were measured to study the cylinder-to-cylinder variations. The measurements were recorded after the in-cylinder pressure and the exhaust gas temperature of all six cylinders stabilized. The data for 120 engine cycles were recorded and the parameters of interest in one case were calculated with different sample sizes to ensure the statistical significance of the sample size.

Fig. 5a and b compare the in-cylinder pressure and integrated apparent rate of heat release (aRoHR) at TP1 on pure diesel (TP1-MEF0) and in DMDF mode (TP1-MEF40). Cylinder pressure measured in C_2 and C_6 were quite similar on pure diesel. However, with 40% MEF, the average peak pressure in C_6 was around 26 bar higher than that in C_2 , also showing an advanced combustion. Moreover, the integrated aRoHR of the two cylinders shows around 12% higher heat release in C_6 than in C_2 in DMDF mode. This suggests that more methanol ends up in the last cylinder, leading to a more severe pressure rise and a higher chance of knocking in C_6 . It was also observed that the cycle-to-cycle variations are increased when running on DMDF mode. The coefficient of variation (COV) of peak cylinder pressure in C_2 and C_6 was 0.6% and 0.5% in MEF0, which increased to 1.4% and 2.5% in MEF40, respectively.

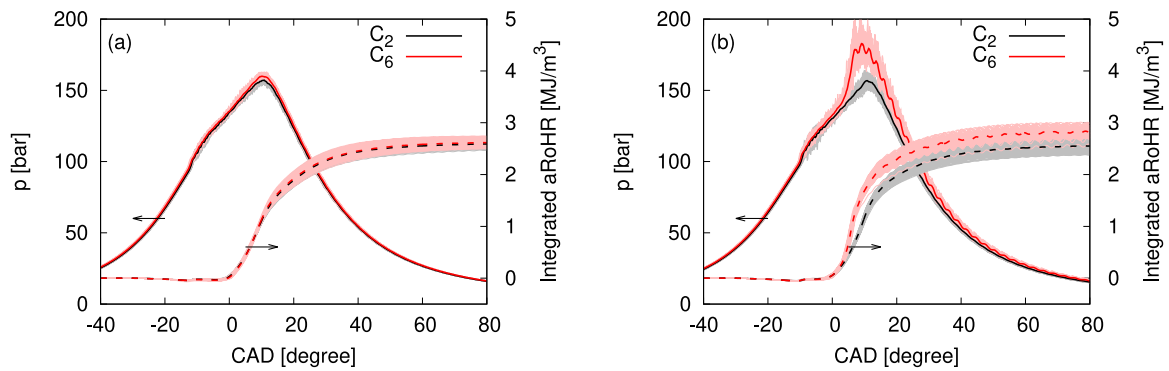


Fig. 5. Experimental measurements of average cylinder pressure and integrated apparent rate of heat release at (a) TP1-MEF0 and (b) TP1-MEF40. The bright colors show all the data recorded in 120 cycles and the dark lines are the average of all cycles. (For interpretation of the references to color in this figure legend, the reader is referred to the web version of this article.)

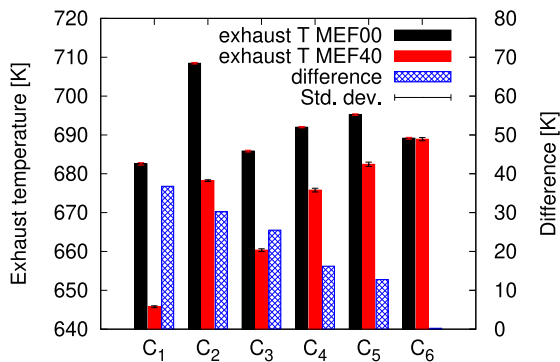


Fig. 6. Comparison of the exhaust gas temperature of different cylinders in TP1-M00 and TP1-M40. Error bars show the standard deviations of the data acquired during more than 60 s of measurement.

Pressure sensors were not available on other cylinders, thus direct comparison of heat release in each cylinder was not possible. However, the cylinder-to-cylinder variation caused by port-fuel injection of methanol can be observed in the exhaust gas temperature of the six cylinders. Fig. 6 presents the exhaust gas temperature of each cylinder when running on pure diesel and DMDF modes, along with the difference between the two modes.

In general, the exhaust temperature of all cylinders is lower in DMDF mode, attributed to the cooling effect of methanol due to its high heat of evaporation. Simple calculations presented in the Appendix show that in this case, evaporation of methanol can cool down the charge temperature up to around 26 °C, which is comparable to earlier reports [27]. However, according to Fig. 6, the difference between the exhaust gas temperatures of the two modes is lower in downstream cylinders. This also suggests that more fuel ends up in the last cylinders due to the asymmetric shape of the inlet manifold, leading to a higher heat release which counteracts the cooling effect of the methanol.

The issue of cylinder-to-cylinder variations was consistently observed across almost every test point during DMDF mode operation. Fig. 7 illustrates the difference in peak cylinder pressure between C₆ and C₂ at different MEF values for TP1 and TP2. In most cases, a higher MEF resulted in a greater difference between the peak pressures. The slight decrease in the difference between TP2-MEF20 and MEF40 can be attributed to experimental uncertainties.

Across all cases, both peak pressure and maximum PRR — hence, knock intensity — in C₆ were higher than in C₂. This higher knock intensity in C₆ limits the utilization of methanol in the engine. Therefore, addressing cylinder-to-cylinder variations caused by port-fuel injection is crucial to maximize the MEF. Consequently, this study focuses on im-

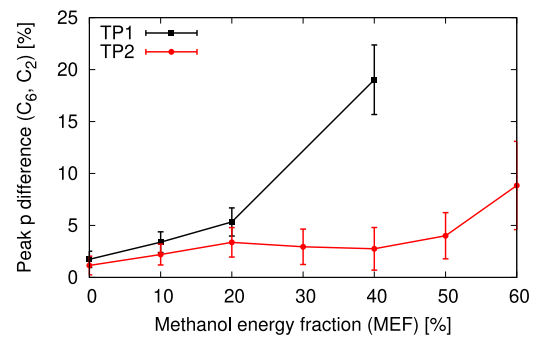


Fig. 7. Experimental results showing the difference in the peak pressure measured in C₂ and C₆ at different MEF values and operating conditions. The error bars show the standard deviation of the values during the 120 cycles of recorded measurements.

proving the inlet manifold design and methanol PFI system to minimize cylinder-to-cylinder variation.

In this study, CFD simulations were employed to visualize and comprehend the methanol flow inside the inlet manifold with the aim of reducing cylinder-to-cylinder variations. To validate the CFD model, experiments were conducted in an optical spray chamber, which are discussed in the following section

4.2. Spray tests and model validation

The spray tip velocity and injection delay of the port fuel injectors hold significant importance for the simulations conducted in this study. These parameters are particularly crucial as the model must accurately predict the amount of fuel reaching the valves before the inlet valve closing (IVC). To measure these parameters, shadowgraphy experiments were conducted in the spray chamber under various conditions, including different pressures, injection durations, and fuel temperatures.

The injection pressure (IP) ranged from 4 to 8 bar, while the chamber pressure (CP) varied from 1 to 4 bar, encompassing the possible range of PFI pressure and the inlet manifold pressure, under boosted conditions of the heavy-duty engine. Injection duration spanned from 2 to 12 ms, and fuel temperature ranged from 25 to 50 °C. The fuel temperature within this range was found to have a negligible effect on the parameters of interest, so it is not further discussed here.

For each case, the spray shadow images underwent post-processing to measure the spray tip penetration at each frame. A mask was utilized to eliminate the opaque parts of the spray chamber from the image, followed by the removal of background noise. Subsequently, the image was converted to a binary image to facilitate identification of the spray tip penetration.

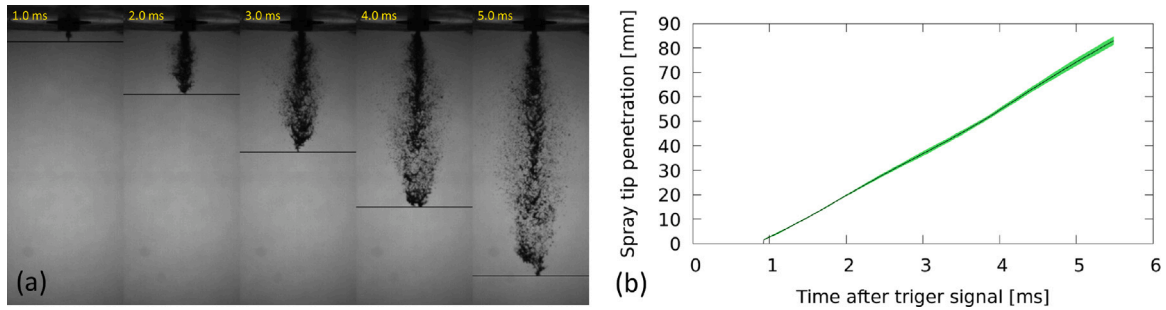


Fig. 8. Experimental results at injection and chamber pressure of 8 and 3 bar, respectively. (a) Raw images from spray chamber and the detected spray tip penetration. (b) Plot of the spray tip penetration versus time.

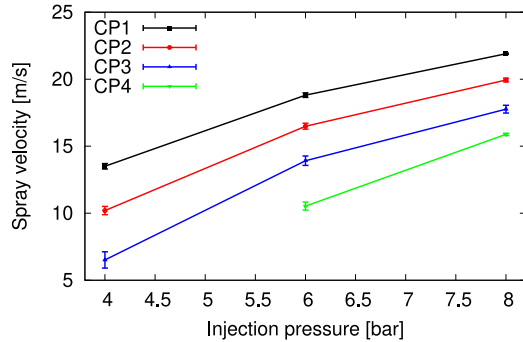


Fig. 9. Spray velocities measured at different injection pressures. CP1 to CP4 refers to chamber pressure of 1 to 4 bar, respectively. The error bars show the standard deviations for five repetitions of each experiment.

As an illustration, Fig. 8a showcases the raw images marked with the spray tip penetration for an injection pressure of 8 bar and chamber pressure of 3 bar. Fig. 8b presents the plot of the spray tip penetration versus time after trigger signal for the same case, with the green shaded area indicating the standard deviation for five repetitions of the experiment.

For all spray tests, an approximate delay of 0.85 ms was observed before the spray became visible in the chamber. Additionally, the spray tip exhibited nearly constant velocity along the length of the chamber (8 cm). Fig. 9 illustrates the average spray velocities calculated from spray tip positions at different injection and chamber pressures (CP).

The average fuel flow rate, spray tip velocity, and the nozzle diameter (1.75 mm) were utilized to estimate the nozzle discharge coefficient (c_d) and velocity coefficient (c_v) for incorporation into the numerical model. In this study, values of $c_d = 0.215$ and $c_v = 0.62$ were employed in the simulations to replicate the same fuel flow rate as a function of pressure.

A stationary spray chamber with identical dimensions to the experiments was simulated with a single injection of methanol. The objective was to tune the spray model and validate the spray tip velocity at different pressures. The CFD predictions of the spray tip penetration over time at four different pressures were compared to the corresponding experimental data in Fig. 10. The same settings were subsequently employed in the next section to model the methanol sprays inside the inlet manifold of the engine.

4.3. Numerical simulations of inlet manifold

This section presents simulation results of the PFI system in both Design 1 and Design 2, as depicted in Fig. 3. The focus is on TP1 from Table 2, which exhibited the highest cylinder-to-cylinder variation. In these simulations, the primary objective is to model the air and methanol flow inside the inlet manifold to determine the distribution

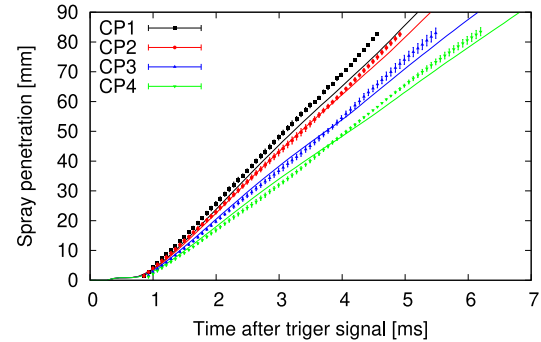


Fig. 10. Comparison of experimental measurements (symbols with error bars) and numerical predictions (lines) of the spray tip penetration at an injection pressure of 8 bar and different chamber pressures. CP1 to CP4 refers to chamber pressure of 1 to 4 bar, respectively.

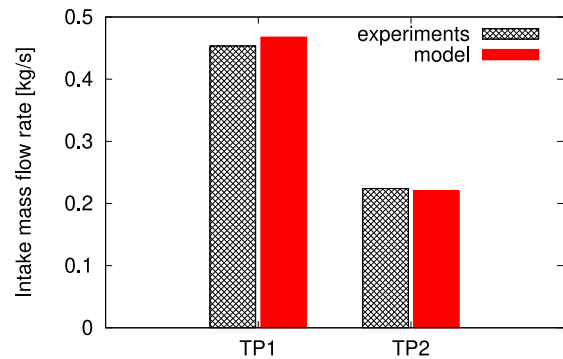


Fig. 11. Modeled mass flow rate at the intake of the engine compared to the experimental data at TP1 and TP2.

of methanol to each cylinder. Therefore, besides validating the spray model presented in the previous section, it is crucial to validate the air flow rate as well.

Each simulation is conducted for five full cycles of the four-stroke engine, spanning from -720 to 2880 CAD of C_2 to achieve steady-state conditions. In all simulations, parameters such as engine speed, compression ratio, intake pressure and temperature, and exhaust pressure are set according to experimental data. The average intake mass flow rate obtained from the simulations is compared to the experimental data for TP1 and TP2, as illustrated in Fig. 11. In both cases, the error between the model predictions and the experiments is below 3%. Moreover, we have estimated the trapped in-cylinder mass based on Yun and Mirsky [32] for both cylinders, and the results were within the 1% range of the CFD predictions.

The next step is to evaluate the ability of the model to predict parameters relevant to cylinder-to-cylinder variations. In pure diesel

operation, the minor variations are typically caused by uneven trapped in-cylinder mass or differences in cylinder cooling. However, with the introduction of PFI methanol, the primary source of variation between cylinders will likely be the methanol mass in different cylinders, which will be the focus of the following analysis.

In CFD simulations, we can calculate the total mass of methanol that passes through the intake ports of each cylinder. Although it is not feasible to directly measure the same parameter in experiments, we can estimate the differences in methanol mass in C_2 and C_6 based on the integrated apparent heat release rate of the two cylinders. The heat release is selected here because it is much more sensitive to the fuel mass compared to other parameters such as the in-cylinder trapped mass.

The total chemical heat release in C_2 in each cycle, $Q_{\text{tot},2}$, can be calculated as

$$Q_{\text{tot},2} = Q_{D,2} + Q_{M,2} = Q_{\text{app},2} + Q_{\text{loss},2}, \quad (6)$$

where $Q_{D,2}$ is the total heat release from diesel, $Q_{M,2}$ is the total heat release from methanol, $Q_{\text{app},2}$ is the apparent heat release (based on pressure trace), and $Q_{\text{loss},2}$ is heat loss in C_2 . The same relations hold for C_6 as well.

Assuming complete combustion, we can express the total heat release from methanol in C_2 as

$$Q_{M,2} = m_{M,2} \cdot LHV_M = Q_{\text{app},2} + Q_{\text{loss},2} - Q_{D,2}, \quad (7)$$

where $m_{M,2}$ is the mass of methanol in C_2 and LHV_M is the lower heating value of methanol.

Using similar relations for C_6 , we obtain

$$Q_{M,6} - Q_{M,2} = Q_{\text{app},6} - Q_{\text{app},2} + [Q_{\text{loss},6} - Q_{\text{loss},2} - (Q_{D,6} - Q_{D,2})]. \quad (8)$$

Since the same amount of diesel is injected into all cylinders, we have $Q_{D,6} = Q_{D,2}$. By substituting from Eq. (7), we obtain

$$m_{M,6} - m_{M,2} = \frac{Q_{\text{app},6} - Q_{\text{app},2} + \delta Q_{\text{loss}}}{LHV_M}, \quad (9)$$

where $\delta Q_{\text{loss}} = Q_{\text{loss},6} - Q_{\text{loss},2}$ is the difference between the heat losses from the two cylinders, which can be estimated based on pure diesel operation.

In pure diesel operation, we have $Q_{M,2} = 0$, and from Eq. (7), we get:

$$\begin{aligned} \delta Q_{\text{loss}} &= [Q_{D,6} - Q_{D,2} - (Q_{\text{app},6} - Q_{\text{app},2})]_{\text{MEF}=0} \\ &= [Q_{\text{app},2} - Q_{\text{app},6}]_{\text{MEF}=0}. \end{aligned} \quad (10)$$

Therefore, to estimate δQ_{loss} , we can calculate the difference between the apparent heat release in the two cylinders at $\text{MEF} = 0$ and assume that the heat loss does not change significantly in other cases. This assumption is valid at low MEF values, and at high MEF can be justified based on the small magnitude of δQ_{loss} compared to $(Q_{\text{app},6} - Q_{\text{app},2})$.

Based on the above calculations, we estimated the difference in the mass of methanol in C_2 and C_6 and compared the results to the numerical simulations of Design 1 in Fig. 12. As MEF increases, the methanol mass imbalance initially increases linearly, then exponentially at higher MEFs. The model predictions for the trend and the values of mass imbalance agree well with the experiments as presented in Fig. 12. However, a perfect match between the model and experiment was not expected because of the various uncertainties in the calculations based on the experimental data.

Various factors contribute to the uncertainty of the calculated difference in methanol mass. For instance, assumptions made in aRoHR calculation, standard deviation of the integrated aRoHR, and estimation of the Q_{loss} based on aRoHR. However, since Eq. (9) only calculates the differences between the two cylinders, a portion of the calculation errors is mitigated through subtraction.

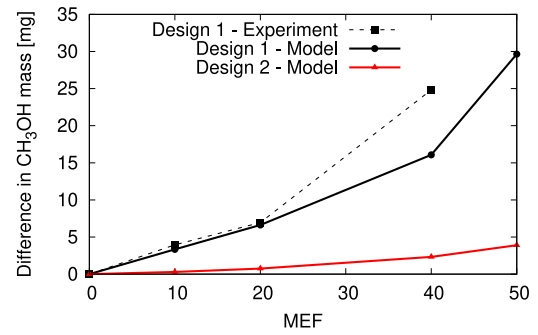


Fig. 12. Methanol mass imbalance between C_2 and C_6 as a function of MEF on TP1. Comparison of experimental and numerical results for Design 1 and numerical results for Design 2.

The modeling results presented in Fig. 12 also indicate that Design 2 exhibits a significantly lower imbalance in methanol distribution. In the following sections, we utilize the simulation results to explain the primary differences between the two designs.

Based on the numerical simulations, both liquid and gas phase methanol can flow toward cylinders other than the target cylinder. A major issue with Design 1 is the tendency for liquid droplets to drift away with the airflow, ultimately moving toward the last cylinders. In Fig. 13a, methanol droplets near the start (CAD = -281) and end (CAD = -161) of injection are depicted. At the beginning of injection, droplets are injected into the inlet manifold with relatively high momentum. Additionally, the inlet valve of C_2 is open, directing airflow toward C_2 , aiding the injected methanol to reach the intended cylinder. However, toward the end of injection, particles are injected with a lower momentum, when C_4 inlet valves are also open, causing methanol to move toward subsequent cylinders.

The scenario differs in Design 2, as shown in Fig. 13b. Here, there is no axial flow inside the added cylindrical pipes, preventing droplets from being washed away by airflow as in Design 1. However, this does not result in a flawless design without cylinder-to-cylinder variations, as a portion of the evaporated methanol will still end up in the last cylinders, as explained in the following.

The issue of spray droplets drifting with the airflow in Design 1 can be elucidated by examining the gas phase velocity near the C_2 ports and the valve timings illustrated in Fig. 14. In this depiction, U and V represent the gas velocity along the x and y axes, respectively (shown in Fig. 3). The start and end of injection (SOI and EOI) for C_2 are highlighted within a shaded blue area in the graph. In addition to the intake valve opening and closing (IVO and IVC) of C_2 , the IVC of C_6 and the IVO of C_4 are also marked in this figure, as they influence the airflow near the C_2 port.

The optimal injection timing falls after IVC₆ and before IVO₄, as during this brief interval, only the C_2 intake valves are open, facilitating the fuel's passage to the correct cylinder with the assistance of the air flow. However, the span between IVC₆ and IVO₄ is merely 35 CAD, whereas the injection duration for TP1-MEF50 is 119 CAD. Consequently, any fuel injected before IVC₆ or after IVO₄ might be subject to drift by the airflow due to the relatively high U and low V during that period. This effect becomes more pronounced in higher MEFs owing to the extended injection duration, or higher speeds due to shorter valve opening durations.

Fig. 15a and b depict the mass fraction of gaseous methanol over a horizontal plane at the middle of the inlet manifold for Designs 1 and 2, respectively. Both images correspond to the fifth cycle of the simulation, during methanol injection toward C_2 . In Design 1, a significant amount of evaporated methanol from previous cycles accumulates at the end of the inlet manifold. This accumulated fuel is eventually drawn into C_5 or C_6 when their inlet valves open. A similar phenomenon occurs in Design 2 (Fig. 15b), but the accumulated

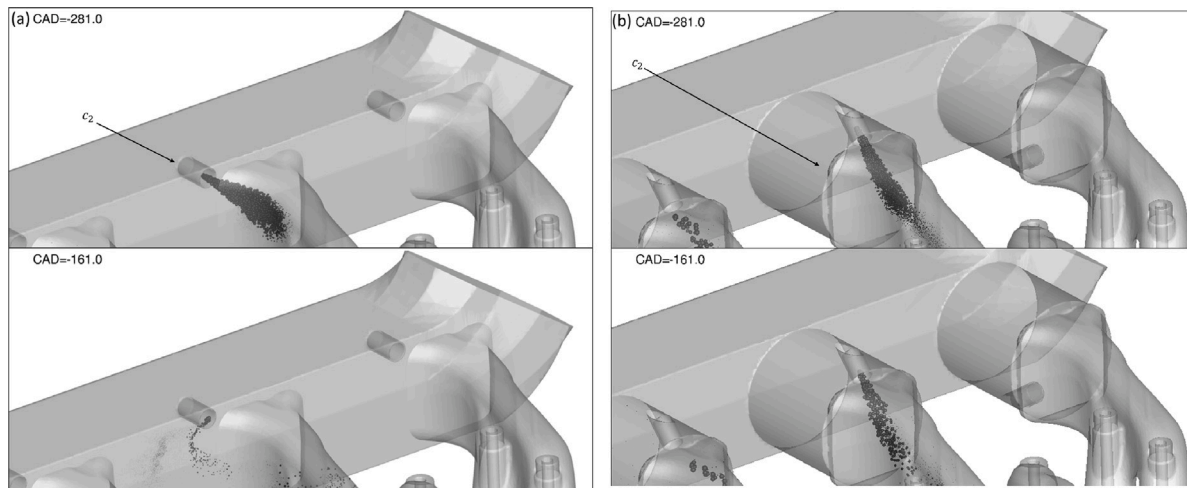


Fig. 13. Comparison of the methanol droplets flow during injection to C_2 in (a) Design 1 and (b) Design 2, at TP1-MEF50.

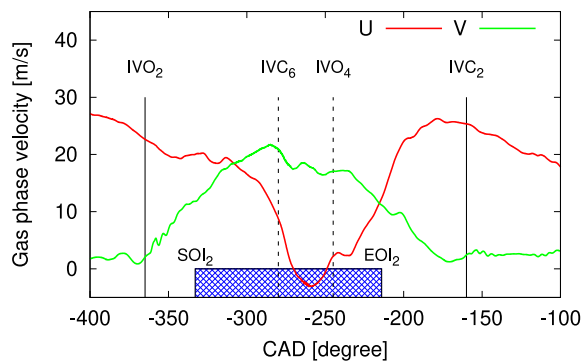


Fig. 14. Gas phase velocity inside the inlet manifold of Design 1, in front of the intake port of C_2 . Injection timing of TP1-MEF50 is marked with the blue shaded area and valve timing of C_2 , C_4 , and C_6 are marked with vertical lines.

methanol near the C_5 and C_6 intake ports is lower. As a result, some imbalance in fuel delivery is expected in Design 2, despite the liquid droplets being directly aimed at each cylinder port. This imbalance explains the slight cylinder-to-cylinder variation observed in Design 2, as it was shown in Fig. 12.

4.4. Parameter study

Based on the findings from the preceding section, Design 2 seems to effectively minimize cylinder-to-cylinder variations. Nonetheless, relocating the inlet manifold and incorporating new connector pipes might present challenges or prove infeasible for certain engines. Hence, understanding the influence of various parameters on methanol mass imbalance in Design 1 is crucial. In this section, numerical simulations of the TP1-MEF50 case were conducted to examine the effects of SOI timing, injection duration, and nozzle location on fuel distribution. These parameters were found to have a significant impact on PFI performance and they were not investigated in earlier studies.

The impact of injection timing on fuel mass imbalance is depicted in Fig. 16a, with SOI timing presented relative to the original case. It was observed that delaying injection aggravates the mass imbalance. Conversely, advancing injection, up to approximately 30 CAD, mitigates fuel mass imbalance. This phenomenon can be rationalized by the timings illustrated in Fig. 14. Advancing injection timing up to about 30 CAD reduces the issues related to droplet drift at EOI, thereby reducing the likelihood of fuel moving toward other cylinders. However, an SOI at -40 CAD does not yield further improvement in mass imbalance, and

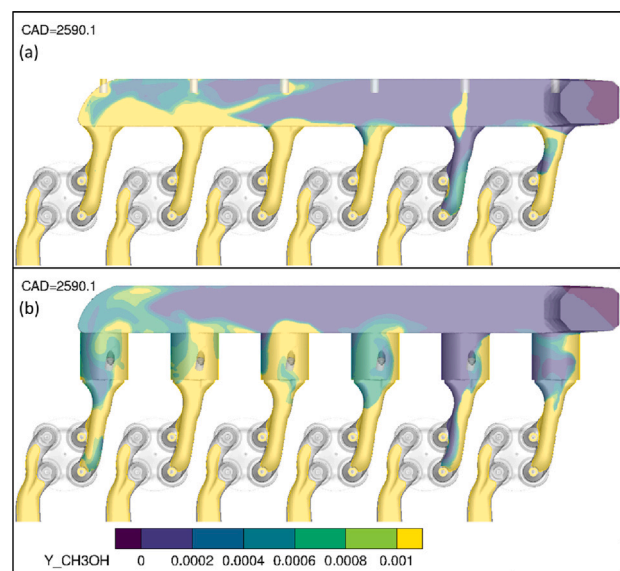


Fig. 15. Distribution of the methanol mass fraction inside the inlet manifold at the fifth cycle of simulation of TP1-MEF50 in (a) Design 1 and (b) Design 2.

earlier SOI timings are impractical as they occur before IVO. Notably, the effect of injection timing appears to be less pronounced compared to the subsequent two parameters discussed.

Another factor impacting the uneven fuel distribution is the duration of fuel injection, as shown in Fig. 16b. The injection pressure required to deliver the same amount of fuel within the desired time-frame is also illustrated in the same figure. In both the original setup and the experiments, the PFI pressure was set at 8 bar, resulting in an injection duration of 119 CAD for this case. CFD results indicate that shortening the injection duration to 80 CAD reduces the fuel imbalance to less than half compared to the original case. Conversely, extending the injection duration to 140 CAD nearly doubles the fuel imbalance relative to the original configuration.

Lastly, the impact of the nozzle tip location on the mass imbalance is examined, with results displayed in Fig. 16c. The inlet manifold measures 8 cm wide, and in the experiments, the nozzle tips of the injectors were positioned 2 cm inside the inlet manifold (6 cm away from the intake ports). Further adjustment of the injectors toward the intake ports was not feasible due to certain connections affixed to the side of the injectors. Nonetheless, nozzle location emerges as the

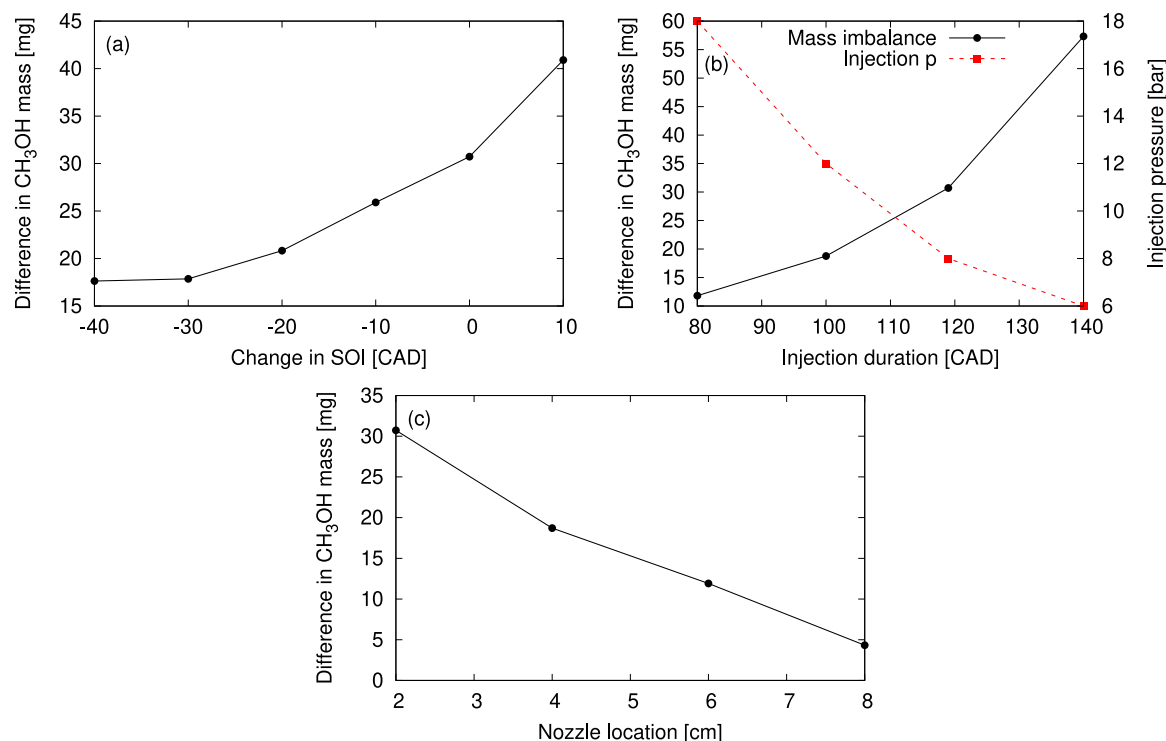


Fig. 16. Effect of different parameters on the fuel mass imbalance between C_2 and C_6 in Design 1, TP1-MEF50. Effect of methanol SOI (a), injection duration (b), and injector nozzle depth in the manifold (c).

most influential parameter under study, warranting consideration in future investigations whenever feasible. In the optimal scenario with the nozzle tip positioned adjacent to the intake ports of the cylinders (location = 8 cm), the difference in fuel mass between C_2 and C_6 is under 5 mg, similar to that observed in Design 2.

The findings from our experiments align with prior studies, reinforcing the crucial role of the PFI system in addressing cylinder-to-cylinder variations and maximum MEF in a methanol-fumigated CI engine [24, 27]. Our numerical simulations contribute to filling the knowledge gaps, explaining how these variations stem from uneven fuel distribution and proposing methods to enhance fuel delivery in the inlet manifold. Yet, there remains ample opportunity for further exploration in this field. Future research could entail experimental validation of Design 2 to assess its efficacy in practical settings. Exploring various diesel injection strategies can help to expand the engine capabilities in DMDF operation. Additionally, developing a CFD model to analyze dual-fuel combustion within a cylinder could offer deeper insights into engine performance and emissions at different conditions.

5. Conclusions

This study concerns retrofitting a 6-cylinder, 13-litre, non-EGR marine diesel engine for DMDF mode, focusing on cylinder-to-cylinder variations. Experimental and numerical investigations were carried out to study the PFI system and methanol distribution which led to the following conclusion:

- Experimental data at high load and MEF (TP1-MEF40) show that the peak pressure and integrated aRoHR in C_6 can exceed those in C_2 by 12% and 16%, respectively. This results in a higher PRR and an increased knock intensity in C_6 , which limits the further replacement of diesel with methanol.
- CFD simulations indicate that the higher peak pressure and heat release in C_6 are caused by uneven methanol distribution. As MEF increases, the disparity in methanol mass distribution becomes more pronounced. At TP1-MEF40, C_6 was predicted to contain 12% more methanol than C_2 .

- A redesigned inlet manifold, feasible for engine retrofitting, was proposed. Simulations demonstrate that the new design reduces the methanol mass imbalance from 12% to 2% compared to the original design. In this improved configuration, liquid methanol more accurately reaches the intended intake port, with the remaining imbalance attributed to evaporated methanol returning to the manifold.
- CFD results show that injection timing, injection duration, and nozzle location all influence methanol mass distribution. Among these, nozzle location proved to be the most impactful, with the potential to reduce up to 75% of the methanol mass imbalance.

CRedit authorship contribution statement

Seyed Morteza Mousavi: Writing – original draft, Validation, Methodology, Investigation, Formal analysis, Conceptualization. **Srinibas Tripathy:** Writing – review & editing, Investigation, Conceptualization. **Patrik Molander:** Writing – review & editing, Project administration, Funding acquisition. **Petter Dahlander:** Writing – review & editing, Supervision, Project administration, Funding acquisition.

Declaration of Generative AI and AI-assisted technologies in the writing process

During the preparation of this work the author(s) used OpenAI's ChatGPT in order to improve the readability of some paragraphs in the text. After using this tool/service, the author(s) reviewed and edited the content as needed and take(s) full responsibility for the content of the publication.

Declaration of competing interest

The authors declare that they have no known competing financial interests or personal relationships that could have appeared to influence the work reported in this paper.

Acknowledgments

This paper is a part of CoMeBust-Me project, which received funding from Vinnova, ScandiNAOS AB, Swedish Maritime Administration, Proman AG (PAG), and Methanol Institute (MI). The authors would like to express their sincere gratitude to Anders Mattsson, Fredrik Derman, and Gudni Gunnarsson for their assistance in performing the experiments, and Prof. Mats Andersson for his support in spray test preparation. The computations were enabled by resources provided by the National Academic Infrastructure for Supercomputing in Sweden (NAISS), partially funded by the Swedish Research Council through grant agreement no. 2022-06725.

Appendix. Effect of methanol PFI on charge cooling

Assuming an adiabatic process of methanol evaporation and mixing with air, the following relation stands:

$$\dot{Q}_1 + \dot{Q}_2 + \dot{Q}_3 = 0, \quad (\text{A.1})$$

where

$$\dot{Q}_1 = \dot{m}_{air} c_{p,air} (T_1 - T_3), \quad (\text{A.2})$$

is the heat released due to air cooling, and

$$\dot{Q}_2 = \dot{m}_M c_{p,M} (T_2 - T_3), \quad (\text{A.3})$$

is the heat release from methanol cooling. In the above equations, T_1 is the initial temperature of the air in the inlet manifold, T_2 is the initial temperature of the fuel when injected into the manifold, and T_3 is the final temperature of the mixture. \dot{m} is the mass flow rate, c_p is the specific heat capacity, and subscripts *air* and *M* correspond to air and methanol, respectively. The last parameter in Eq. (A.1), is the evaporation heat of methanol calculated as

$$\dot{Q}_3 = -\dot{m}_M h_{fg,M}, \quad (\text{A.4})$$

where $h_{fg,M}$ is the specific heat of evaporation for methanol evaporation. Assuming constant properties and considering the measured air and methanol flow rates, the air temperature drops 26 K in the TP1-MEF40 case.

Data availability

Data will be made available on request.

References

- [1] Yao C, Pan W, Yao A. Methanol fumigation in compression-ignition engines: A critical review of recent academic and technological developments. *Fuel* 2017;209:713–32.
- [2] Verhelst S, Turner JW, Sileghem L, Vancoillie J. Methanol as a fuel for internal combustion engines. *Prog Energy Combust Sci* 2019;70:43–88.
- [3] Saxena MR, Maurya RK, Mishra P. Assessment of performance, combustion and emissions characteristics of methanol-diesel dual-fuel compression ignition engine: A review. *J Traffic Transp Eng (Engl Ed)* 2021;8(5):638–80.
- [4] Svanberg M, Ellis J, Lundgren J, Landälv I. Renewable methanol as a fuel for the shipping industry. *Renew Sustain Energy Rev* 2018;94:1217–28.
- [5] Shukla PC, Belgioorno G, Di Blasio G, Agarwal AK. Alcohol as an alternative fuel for internal combustion engines. Springer; 2021.
- [6] Coulier J, Verhelst S. Using alcohol fuels in dual fuel operation of compression ignition engines: a review. In: 28th CIMAC world congress on combustion engine. CIMAC; 2016, p. 1–12.
- [7] Ning L, Duan Q, Kou H, Zeng K. Parametric study on effects of methanol injection timing and methanol substitution percentage on combustion and emissions of methanol/diesel dual-fuel direct injection engine at full load. *Fuel* 2020;279:118424.
- [8] Xu L, Treacy M, Zhang Y, Aziz A, Tuner M, Bai X-S. Comparison of efficiency and emission characteristics in a direct-injection compression ignition engine fuelled with iso-octane and methanol under low temperature combustion conditions. *Appl Energy* 2022;312:118714.
- [9] Zhao F-Q, Lai M-C, Harrington DL. The spray characteristics of automotive port fuel injection—a critical review. *SAE Trans* 1995;399–432.
- [10] Yao C, Cheung CS, Cheng C, Wang Y. Reduction of smoke and NOx from diesel engines using a diesel/methanol compound combustion system. *Energy Fuels* 2007;21(2):686–91.
- [11] Cheng C, Cheung CS, Chan TL, Lee S, Yao C. Experimental investigation on the performance, gaseous and particulate emissions of a methanol fumigated diesel engine. *Sci Total Environ* 2008;389(1):115–24.
- [12] Imran A, Varman M, Masjuki HH, Kalam MA. Review on alcohol fumigation on diesel engine: a viable alternative dual fuel technology for satisfactory engine performance and reduction of environment concerning emission. *Renew Sustain Energy Rev* 2013;26:739–51.
- [13] Cheung CS, Cheng C, Chan TL, Lee S, Yao C, Tsang K. Emissions characteristics of a diesel engine fueled with biodiesel and fumigation methanol. *Energy Fuels* 2008;22(2):906–14.
- [14] Yao C, Cheung CS, Cheng C, Wang Y, Chan TL, Lee S. Effect of diesel/methanol compound combustion on diesel engine combustion and emissions. *Energy Convers Manage* 2008;49(6):1696–704.
- [15] Zhang Z, Cheung CS, Chan TL, Yao C. Emission reduction from diesel engine using fumigation methanol and diesel oxidation catalyst. *Sci Total Environ* 2009;407(15):4497–505.
- [16] Cheung CS, Zhang Z, Chan TL, Yao C. Investigation on the effect of port-injected methanol on the performance and emissions of a diesel engine at different engine speeds. *Energy Fuels* 2009;23(11):5684–94.
- [17] Pan W, Yao C, Han G, Wei H, Wang Q. The impact of intake air temperature on performance and exhaust emissions of a diesel methanol dual fuel engine. *Fuel* 2015;162:101–10.
- [18] Wang Q, Wei L, Pan W, Yao C. Investigation of operating range in a methanol fumigated diesel engine. *Fuel* 2015;140:164–70.
- [19] Wang Q, Wang B, Yao C, Liu M, Wu T, Wei H, Dou Z. Study on cyclic variability of dual fuel combustion in a methanol fumigated diesel engine. *Fuel* 2016;164:99–109.
- [20] Kumar D, Sonawane U, Chandra K, Agarwal AK. Experimental investigations of methanol fumigation via port fuel injection in preheated intake air in a single cylinder dual-fuel diesel engine. *Fuel* 2022;324:124340.
- [21] Duraisamy G, Rangasamy M, Nagarajan G. Effect of EGR and premixed mass percentage on cycle to cycle variation of methanol/diesel dual fuel RCCI combustion. Technical report, SAE Technical Paper; 2019.
- [22] Wei L, Yao C, Han G, Pan W. Effects of methanol to diesel ratio and diesel injection timing on combustion, performance and emissions of a methanol port premixed diesel engine. *Energy* 2016;95:223–32.
- [23] Agarwal AK, Kumar V, Jena A, Kalwar A. Fuel injection strategy optimisation and experimental performance and emissions evaluation of diesel displacement by port fuel injected methanol in a retrofitted mid-size genset engine prototype. *Energy* 2022;248:123593.
- [24] Chen Z, Yao C, Yao A, Dou Z, Wang B, Wei H, Liu M, Chen C, Shi J. The impact of methanol injecting position on cylinder-to-cylinder variation in a diesel methanol dual fuel engine. *Fuel* 2017;191:150–63.
- [25] Xu C, Zhuang Y, Qian Y, Cho H. Effect on the performance and emissions of methanol/diesel dual-fuel engine with different methanol injection positions. *Fuel* 2022;307:121868.
- [26] Xu C, Cho H, Park DH. The influence of intake air temperature and varying injection positions on the combustion and emission of CI engine running on methanol. *Int J Appl Eng Technol* 2021;3.
- [27] Dierickx J, Verbiest J, Janvier T, Peeters J, Sileghem L, Verhelst S. Retrofitting a high-speed marine engine to dual-fuel methanol-diesel operation: A comparison of multiple and single point methanol port injection. *Fuel Commun* 2021;7:100010.
- [28] Richards K, Senecal P, Pomraning E. CONVERGE 3.0, Convergent Science, Madison, WI. 2023.
- [29] O'Rourke PJ, Amsden AA. The TAB method for numerical calculation of spray droplet breakup. Technical report, SAE technical paper; 1987.
- [30] Amsden AA, O'Rourke PJ, Butler TD. KIVA-II: A computer program for chemically reactive flows with sprays. Technical report, Los Alamos, NM (United States): Los Alamos National Lab.(LANL); 1989.
- [31] O'Rourke PJ, Amsden A. A spray/wall interaction submodel for the KIVA-3 wall film model. *SAE Trans* 2000;281–98.
- [32] Yun H, Mirsky W. Schlieren-streak measurements of instantaneous exhaust gas velocities from a spark-ignition engine. *SAE Trans* 1974;3143–58.